SAND2020-2754J

Photothermal alternative to device fabrication using atomic precision advanced manufacturing techniques

A. M. Katzenmeyer[a], S. Dmitrovic[b], A. D. Baczewski[a], E. Bussmann[a], T.-M. Lu[a], E. M. Anderson[a], S. W. Schmucker[a], J. A. Ivie[a], D. M. Campbell[a], D. R. Ward[a], G. T. Wang[a], S. Misra*[a]
[a]Sandia National Laboratories, Albuquerque, NM 87185 [b]College of Optical Sciences, University of Arizona, 85721

ABSTRACT

The attachment of dopant precursor molecules to depassivated areas of hydrogen-terminated silicon templated with a scanning tunneling microscope (STM) has been used to create electronic devices with sub-nanometer precision, typically for quantum physics demonstrations, and to dope silicon past the solid-solubility limit, with potential applications in microelectronics and plasmonics. However, this process, which we call atomic precision advanced manufacturing (APAM), currently lacks the throughput required to develop sophisticated applications because there is no proven scalable hydrogen lithography pathway. Here, we demonstrate and characterize an APAM device workflow where STM lithography has been replaced with photolithography. An ultraviolet laser is shown to locally heat silicon controllably above the temperature required for hydrogen depassivation. STM images indicate a narrow range of laser energy density where hydrogen has been depassivated, and the surface remains well-ordered. A model for photothermal heating of silicon predicts a local temperature which is consistent with atomic-scale STM images of the photo-patterned regions. Finally, a simple device made by exposing photo-depassivated silicon to phosphine is found to have a carrier density and mobility similar to that produced by similar devices patterned by STM.

Keywords: photolithography, photothermal effects, hydrogen lithography, surface morphology, nanoscale devices, scanned probe lithography

1. INTRODUCTION

Scanning tunneling microscopy (STM) can be used to incorporate phosphorus dopants at the surface of silicon with +/- 1 lattice site (~ 0.35 nm) precision. This capability has been leveraged to fabricate one-off dopant-based physics demonstrations where proximal devices are used to manipulate the electrons bound to one or a few well-placed phosphorus atoms [1-4]. With the exponentially rising development cost of proceeding to smaller device sizes in microelectronics, leveraging this fabrication flow, which we call APAM, to explore digital microelectronics concepts at the physical limit of atoms can provide an important pathfinding function [5]. However, the complexity of devices that can be made with APAM needs to advance significantly for this to be a possibility, and the underlying process development will require making an unimaginable number of devices with a tool that is notoriously slow. In addition, the APAM process introduces a density of dopants into silicon that exceeds the solid solubility limit, which creates electrical characteristics and optical response [5] that is qualitatively different than what is possible in silicon at conventional levels of doping. Here, potential applications, from enhanced doping in microelectronics to plasmonic devices, do not require atomic precision, but need patterning over larger areas than attainable with STM, and some path to manufacturability.

The only step of the APAM process that has no straightforward translation to scalable processing is hydrogen depassivation lithography. In the APAM process, hydrogen attached to an atomically clean Si(100) surface is selectively depassivated using the STM with sub-nm precision [6]. Dopant precursor molecules, such as phosphine, subsequently introduced into the ultra-high vacuum chamber attach selectively only to the depassivated areas, and not to sites that remain passivated with hydrogen [7]. A modest thermal anneal to temperatures that leave the hydrogen resist mask intact is sufficient to incorporate phosphorus dopants into the lattice. The dopants are then encapsulated with a silicon overlayer to protect them. The encapsulation step must be executed at low enough temperatures to prevent diffusion of the dopants [8]. In terms of manufacturing, the APAM process is thermally compatible for inclusion between the high-temperature process steps

* Corresponding author: Shashank Misra, smisra@sandia.gov, (505) 284-1953

associated with front-end-of-line microelectronics manufacturing, and the low-temperature process steps associated with back-end-of-line [9]. To scale the process, the initial sample preparation and hydrogen termination can be implemented at the wafer scale within a low-pressure chemical vapor deposition tool (LPCVD) [10]. Both precursor dosing and low-temperature silicon encapsulation can, in principle, be implemented in a straightforward way at the wafer scale with a molecular beam epitaxy system and a doping antechamber. In contrast, even at the scale of a single device on one chip, the time to fabricate a device, typically one day, is dominated by the time it takes STM to depassivate hydrogen.

Fortunately, hydrogen depassivation has previously been demonstrated using several methods that are much faster than scanned probe microscopy. Near-surface secondary electrons from a scanning electron microscope (SEM) have been used to remove hydrogen from a passivated surface with a spot-size of around 200 nm [11]. While much faster than scanned probe microscopy, SEM shares the limitation of a serial writing process, as opposed to the parallel writing of many features afforded by photolithography. Mid-infrared light can be used to directly excite the stretching mode of the Si-H bond, but resolution limitations from the wavelength required (4.8 μm) limit the applicability of this mechanism [12]. Direct excitation of the hydrogen from the bonding to the anti-bonding configuration has been demonstrated with 157 nm light [13]. However, optics at vacuum ultraviolet wavelengths are both costly and difficult. At wavelengths between the indirect bandgap for silicon (1100 nm) and the direct electronic excitation (180 nm), light has been used to locally heat silicon above 430° C, the temperature where it will desorb from silicon [14]. This range of wavelengths provides a continuous tradeoff between ease of optics and wavelength-limited feature size.

Here, we fabricate a simple APAM device using a pulsed ultraviolet laser to photothermally desorb hydrogen. Absorption in silicon is strong in the ultraviolet, where photon energies exceed the direct bandgap. We expect 337 nm light to localize heat to within 10 nm of the surface, and pulsing to limit the total energy deposited in the sample. We first show that the atomic nature of the hydrogen resist [15] makes it impervious to dose-related issues that lead to underexposure and over-exposure with conventional photoresists. Next, we use STM imaging to evaluate the suitability of the depassivated regions for the phosphine chemistry required to create a device. We find a narrow range of laser energy density where hydrogen is depassivated without disrupting the structure of the surface [16-18]. A model considering both the intensity of the laser light and the nonlinear heat conduction in the silicon is found to be consistent with the data, which can guide the selection of different lasers for photothermal desorption more generally. Finally, we present magneto-transport data from a van der Pauw structure fabricated using photothermal desorption.

2. METHODS

Samples were cleaned and hydrogen terminated by first flashing to 850° C in ultra-high vacuum (1 x 10^{-10} torr) to remove the surface oxide, followed by passivation using 2 x 10^{-6} torr of atomic hydrogen created by a hot tungsten filament. The samples used for Figures 2, 3, &4 were first prepared with this procedure, then exposed to pulsed laser light. For Figures 2 & 3, the chip was removed to air to form native oxide selectively on depassivated regions, then reinserted into vacuum. An anneal to 300° C removed water physisorbed on the surface, and a subsequent 30 nm silicon cap deposited at the same temperature using a sublimation source was used to preserve the interface. A Nikon optical microscope identifies the contrast created by the buried dielectric in differential interference contrast (DIC) imaging. For Figure 4, STM images were taken after hydrogen depassivation using an Omicron Variable Temperature STM operating at room temperature. Images shown are all recorded at a sample bias of -2.5 V (corresponding to electrons tunneling from the sample to the tip) and with an imaging setpoint of 0.2 nA. The sample used for Figure 6 was fabricated following the procedure found in Ref. [9], with a photothermal process replacing STM-based hydrogen depassivation. Silicon chips with pre-implanted contacts and alignment marks were cleaned, terminated, and photothermally patterned. The sample was then dosed to 20 L of PH_3, which was incorporated at 300° C, and a 30 nm layer of Si at the same temperature grown on top. The samples were contacted by etching vias into the implants and depositing Al metal. Magnetotransport measurments were taken at 4 K in a maximum field of 1 T.

Laser depassivation was performed using a custom scanning laser microscope built to interface to UHV chambers described above via a viewport. A nitrogen (N_2) laser emitting 3.5 ns pulses of 126 μJ at 337.1 nm (bandwidth 0.1 nm) was used with variable focus and attenuation as the illumination source. The laser pulsing was triggered with a function generator to emit from a single pulse to a repetition rate of 100 Hz depending on desired exposure. The beam size exiting the laser aperture was 3 mm x 7 mm with a full angle divergence of 5 mrad x 8 mrad. For this study a 50 mm focal length plano-convex lens or a 13.3 mm effective focal length reflecting objective was used to focus the light onto the sample.

3. RESULTS AND DISCUSSION

3.1 Atomic resist

In contrast to photolithography with conventional resists, the concept of dose loses relevance for photothermal patterning of atomic resists chemically bonded to the surface. For photothermal depassivation, the peak temperature of the silicon surface must exceed the temperature at which hydrogen desorbes from silicon. Below this threshold, no hydrogen is desorbed, and above this threshold, there is no penalty for multiple or extended exposures. Consider Figure 1, a plot of surface temperature as a function of time for two different scenarios. Shown, in red, is a temperature profile resulting from a short laser pulse of sufficient energy density to exceed the desorption temperature, T_{desorb}, of the atomic-layer resist. Fulfilling this condition results in depassivation. In blue, an infinite pulse train is depicted where the peak temperature corresponding to each pulse does not exceed T_{desorb}. As the repetition rate is slow compared to the cooling rate of the sample, the dose cannot accumulate as it would in a conventional photoresist, and no hydrogen is desorbed. Similarly, if carefully tuned, even if the first red pulse depassivates 99% of the hydrogen, the second pulse can remove additional hydrogen without causing any additional deleterious effects. In practice there is no easy way to measure the temperature of just the surface of silicon for the 3.5 ns while it is being irradiated, so, instead, we track the energy density of the laser and later use a photothermal heating model to arrive at a putative temperature.

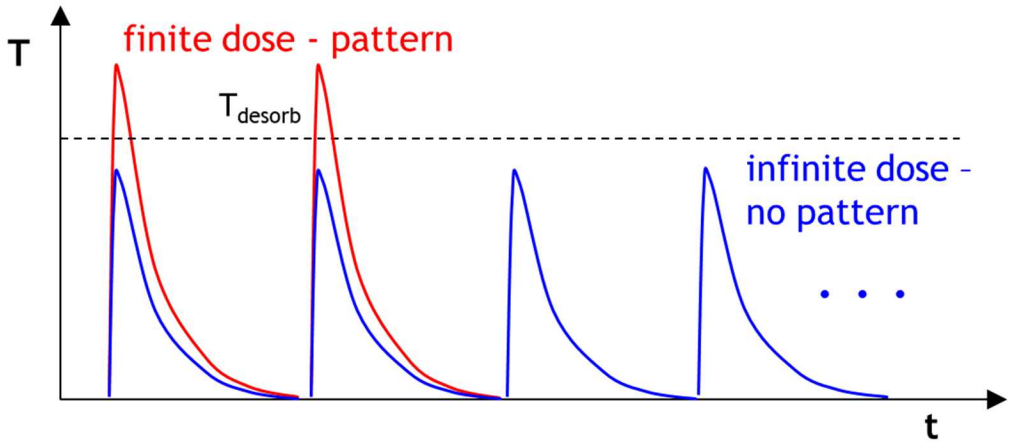

Figure 1: Temporal temperature profiles for a finite dose which patterns the atomic-layer resist (red) and an infinite dose which does not (blue).

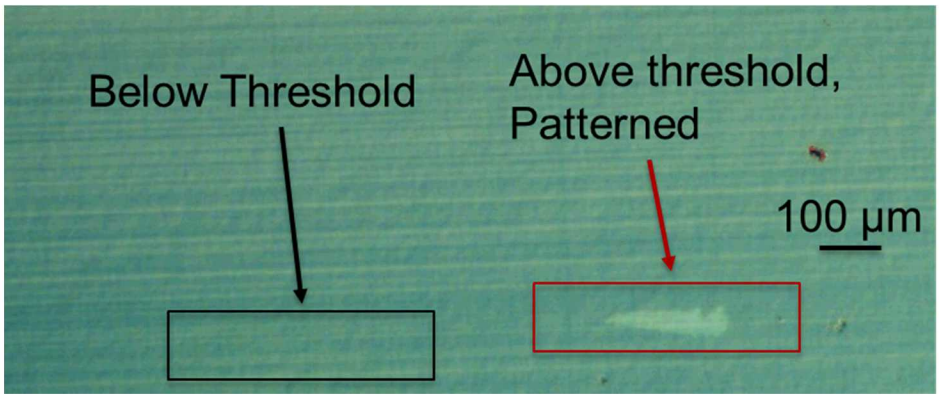

Figure 2: DIC microscopy image of an exposure test sample. The red box contains an oxidized region resulting from above threshold exposure and oxidation. The black box contains a region exposed with insufficient energy density to reach the desorption temperature.

Both the concept of sub-threshold exposure desorbing no hydrogen and multiple above-threshold exposures causing no harm are illustrated in the data of Figures 2 and 3 [15]. Here, we use differential interference optical microscopy to show

the dielectric contrast formed by native oxide formation in depassivated areas of the surface, as described in the Methods section. This is a quick way of narrowing down the large phase space of laser powers and pulse repetitions to favorable ranges that show some depassivation. In Figure 2, the black box indicates a below threshold (below T_{desorb}) exposure where no patterning has occurred. A slight increase in laser power, by 10%, results in hydrogen desorption and native oxide formation in the red box. Unfortunately, systematic errors in the determination of the area of the focused pulse prevent extraction of a threshold energy density for hydrogen depassivation from this data. Figure 3 shows the effect of multiple above-threshold exposures. Despite a comparable energy density in the left panel and the right panel, there is no additional damage being done to the silicon from multiple exposures. Moreover, multiple exposures are seen to reduce pattern roughness that likely results from statistical fluctuations of the light source.

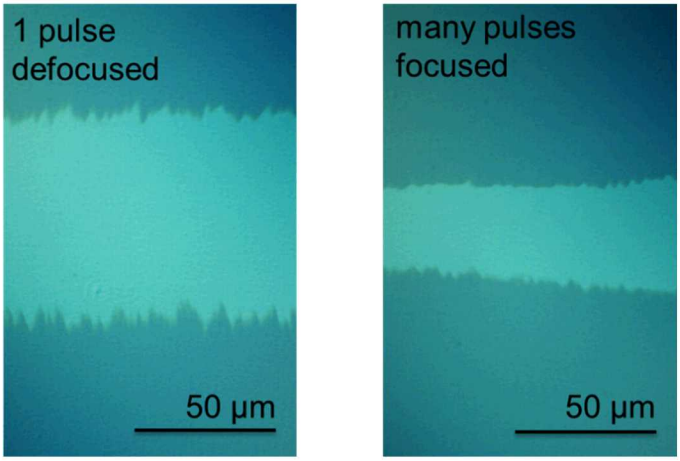

Figure 3: 100x DIC microscopy image of oxidized sample patterned by (left) single laser pulse (76 mJ/cm^2) and (right) many laser pulses (90 mJ/cm^2). Many pulses can potentially reduce edge roughness without overexposure.

3.2 Surface roughening

There is a potentially wide window of surface temperatures where photothermal hydrogen desorption can be expected to be effective. The temperature must be above 430° C to activate desorption of the monohydride termination [14], but below 1400° C to avoid melting [19]. However, for the purposes of making a device using the APAM process flow, this surface must also be suitable for the phosphine chemistry. The requirement that the atomic-scale 2x1 dimer-row surface reconstruction of Si(100) is present may place a significantly tighter constraint on the range of acceptable laser energy density, especially as non-thermal roughening mechanisms may be relevant during a laser pulse.

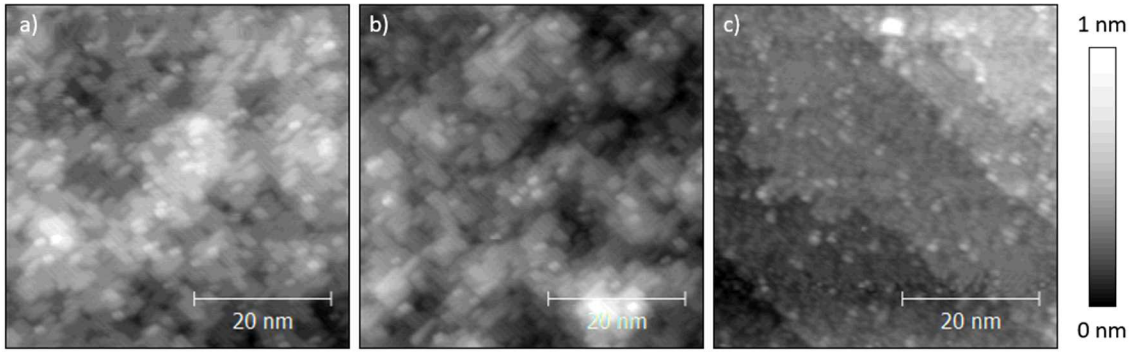

Figure 4: 50 nm x 50 nm STM topography scans of regions exposed with energy densities of (a) 101 mJ/cm^2, (b) 90 mJ/cm^2, and (c) 81 mJ/cm^2. STM lithography in a serpentine pattern was attempted prior to each scan and indicates H was already removed from the surface by laser exposure.

As shown in Figure 4, following exposure with a fluence of 81 mJ/cm^2, a majority of the surface is depassivated while the underlying flat step-terrace surface structure, and the 2x1 dimer rows remain intact. As the laser fluence is increased to 90-100 mJ/cm^2 the surface roughens considerably. While the crystallinity of the surface is preserved, as indicated by the layer-by-layer character of the roughening and the 2x1 dimer rows apparent in the images, such roughening is generally undesirable for atomic-precision device fabrication. As we will show below with a model that treats photothermal heating, these energy densities keep the surface well below its melting point, suggesting that non-thermal mechanisms are responsible for the roughening seen in Figure 4.

3.3 Photothermal heating model

There is a narrow window of laser energy density for which photolithography was measured to be effective. We cannot easily measure the sample surface temperatures, so to assist in determining the laser conditions that are within this window we make use of a physical model for photothermal heating [20]. The form of this model is an inhomogeneous nonlinear heat equation in which the forcing term is due to the incident intensity of the laser beam and the nonlinearity is predominantly due to the temperature-dependence of the thermal conductivity of silicon. Given such a model, it is straight forward to approximately solve for the peak temperature achieved at the end of the pulse in the center of the incident laser beam. If it falls within the window in which photolithography is effective then we deem this a reasonable starting point for an experiment. For the purposes of a proof-of-concept, we have constructed an approximate analytical solution for the peak temperature. We leave a description of a numerical solution of this model to future work.

The peak surface temperature, T_{peak}, at the center of a normally incident symmetric Gaussian pulse with peak intensity, I, and temporal duration, Δ, is approximated as

$$T_{peak} \approx T_{init} + \frac{2I(1-R)}{GM\left[\kappa(T_{init}), \kappa\left(T_{peak}\right)\right]}\sqrt{\frac{GM[D(T_{init}), D\left(T_{peak}\right)]\Delta}{\pi}} + \mathcal{O}\left(\left[\alpha\sqrt{D\Delta}\right]^{-1}\right),$$

where R is the reflectivity of the surface, GM is the geometric mean, κ and D are the temperature-dependent thermal conductivity and diffusivity of silicon, and α is the absorption coefficient of silicon. Because we are using a laser with a photon energy above the direct bandgap of silicon, we can neglect the temperature-dependence of α [21]. We have also assumed that the spot-size is much larger than the length scale for absorption. In fact, the dominant contribution to the peak temperature is independent of both of these length scales, and the leading correction is on the order of the dimensionless product of the absorption coefficient and the root-mean-squared displacement of a packet of thermal energy over the duration of the pulse. In physical terms, this expression is most accurate when the thermal energy deposited in a laser pulse diffuses much further than the length scale over which the optical absorption occurs. In this limit the peak temperature is dominated by the component of the transient response that is independent of the absorption length and spot-size. This is the case for our experiment. We have employed the geometric mean to approximately treat the nonlinearity according to the physical reasoning that during illumination, the peak temperature will increase with the square root of time.

This can be further simplified by treating the specific heat capacity, C_p, and mass density of crystalline silicon, ρ, as independent of temperature and using a power law model for the thermal conductivity [22]. Simple algebraic manipulations render an expression strictly in terms of the temperature-dependent thermal conductivity,

$$T_{peak} \approx T_{init} + 2I(1-R)\sqrt{\frac{\Delta}{\pi\rho C_p GM[\kappa(T_{init}), \kappa\left(T_{peak}\right)]}}.$$

This equation is straight forward to solve numerically.

Figure 5 illustrates the peak surface temperatures predicted using our model for the experiments considered in Figures 3 and 4, where it correctly predicts that the temperature is sufficient for desorption. Because the heating that leads to hydrogen desorption is due to the transient response rather than the steady state, the temperature profile at the peak of the laser pulse follows roughly the same profile as the absorbed power density. Laterally, this means that the surface temperature profile has roughly the same shape as the incident intensity. In depth, the absorbed power density decays exponentially over a length scales set by α. For an ultraviolet laser in silicon, this corresponds to most of the energy being absorbed over fewer than 10 nm.

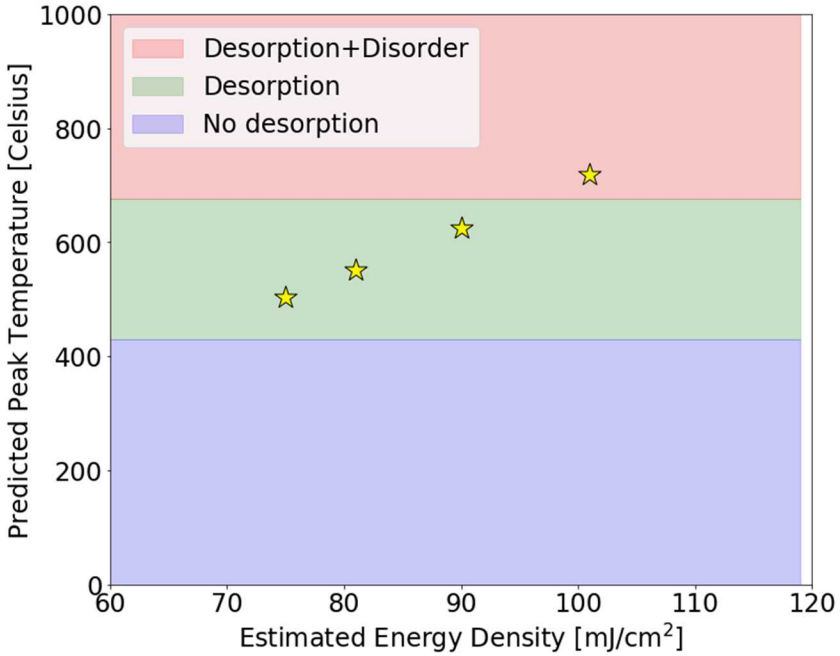

Figure 5: Predicted peak temperatures evaluated using our photothermal heating model for 6 different pulsed energy densities. The different colored regions correspond to whether the peak temperature is below 430°C (no desorption), above 430°C but below 675°C (desorption), or above 675°C (desorption+disorder), with the expected outcomes indicated parenthetically. Not included is a data point for a test at 347 mJ/cm^2 in which melting was observed via optical microscopy. It is evident that our model would predict a peak temperature well above the melting point. But because our model does not account for the latent heat of melting or the different thermal transport properties of the liquid phase, it would not give an accurate temperature estimate.

Interestingly, the surface disorder seen in the data of Figure 4 occurs for temperatures well below thresholds for melting and ablation. Rather, laser-induced modification of solid Si(100)-2x1 surfaces occurs via a non-thermal mechanism: bond scission by electronic excitation [16-18]. Prior works, utilizing 532 nm light, indicate that for fluences < 100 mJ/cm^2, only Si dimers in the outermost atomic layer are desorbed from the surface. In this process, only one atomic layer is involved and the surface retains an overall flat step terrace structure comparable to what we show in Figure 4 (c). As the fluence is increased, Yasui *et al.*, observed that both vacancy and addimer formation are active, leading to island and pit nucleation and roughening [18], similar to what we see in Figures 4 (a,b).

Another feature of our model that requires clarification is the observed efficiency of the photothermal activation of hydrogen desorption. Our model predicts that after the laser pulse is applied the surface temperature will return to ambient on a timescale on the order of picoseconds. Thus we should interpret all desorption as occurring on the nanosecond timescale of the pulse itself. The activation barrier for desorption is sufficiently high that in order for the Arrhenius rate of desorption to approach GHz we will actually require temperatures closer to the melting point of silicon than the quoted 430°C threshold. Based on these observations we expect that the pulsed energy density is actually higher than we are presently estimating. It may also be the case that the mechanism for desorption is more complicated than simple thermal activation. Future work will seek to resolve this.

3.4 APAM-inspired device

Having established a tight window within which photothermal depassivation produces a surface suitable to incorporate phosphine, we now turn to fabrication of a simple van der Pauw device to determine the density of active carriers and their mobility. Many of the interesting electrical and optical properties [5] of APAM systems derive not from the atomic-scale dimensions, but from the active dopant density being an order of magnitude higher than what can be achieved with other

techniques. This level of doping – nearly one in every four atoms at the surface – far exceeds the solid solubility limit. To do this, we have photothermally depassived the hydrogen in the central region of a sample with eight pre-implanted contacts in three overlapping pulses, each of energy density 100 mJ/cm^2 (Figure 6 (a)). The depassivated area was not constrained to be just the central, square area, but is an inchoate region that extends out to the black alignment marks. While unconventional, this permits a measurement of the carrier density and mobility using the Van der Pauw method.

The phosphorus delta layer was electrically characterized at 4 Kelvin, at which the carriers in the substrate freeze out and do not contribute to transport. DC and low-frequency transport measurements were performed in a magnetic field for extracting the density and mobility of the delta layer. The carrier density extracted from the Hall coefficient was 4.8×10^{14} cm^{-2}. A resistivity of 250 Ohm/square was obtained using the Van der Pauw method. From the carrier density and resistivity, we extracted a mobility value of 52 cm^{2}V^{-1}s^{-1}. This mobility value is consistent with typical phosphorus delta layers produced by the conventional APAM method, while the carrier density is approximately three times as high as that of a saturated delta layer. The unconventional geometry of the doped region with respect to the ion implanted contacts can complicate a Van der Pauw measurement. A second possibility is the roughness of the surface in Figure 4 (a) leading to a high effective surface area. However, for an ellipsoidal bump to have triple the surface area of the square it sits in (Figure 6 (b)) requires it to be as tall as it is wide, which is inconsistent with the STM data in Figure 4 (a). While this data is conclusive evidence that APAM works with photolithography replacing STM lithography, additional work needs to be done to understand the origin of the high carrier density.

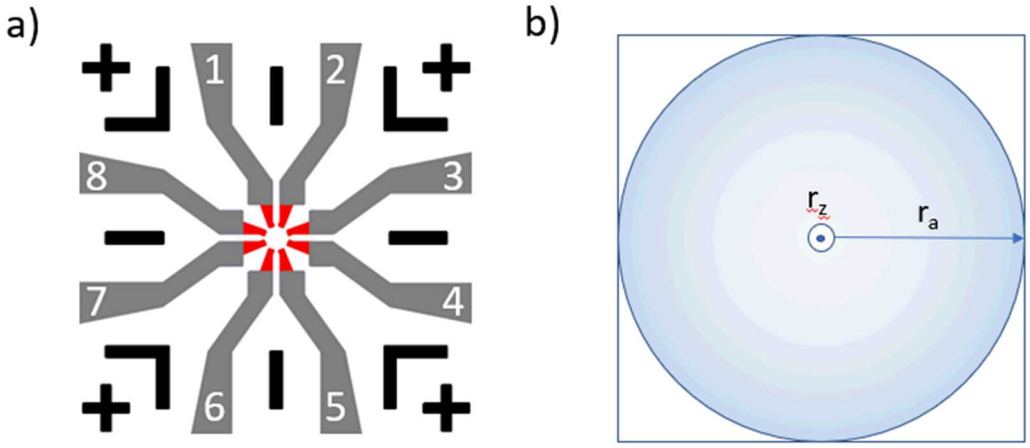

Figure 6: (a) Schematic diagram, overhead view, of the Van der Pauw device. Black objects are tungsten alignment marks, red objects are ion implanted contacts, and grey objects are the aluminum that neck in to the implants. The depassivated region, and hence the phosphorus device, was an irregular region larger than the implants but smaller than the alignment marks. Contacts 1, 3, 5, and 7 were used for the measurement, and the other contacts were left open circuit. (b) Overhead view of a square with an ellipsoidal bump in the middle of it, having a circular cross section with radius r_a and a height r_z. A square with an ellipsoid bump in the middle will have approximately 3 times the surface area of just the square for $r_z \sim 2r_a$.

4. CONCLUSION

In this work, we have shown the viability of photothermal hydrogen lithography to selectively dope parts of the silicon surface using the phosphine chemistry that underlies APAM. For this to open the door both to the rapid fabrication pathway required for process development and applications which leverage ultra-high dopant densities, two issues remain to be resolved. First, Hall bars with the proper geometry need to be fabricated that have the same electrical properties as STM-based APAM. As part of this, the threshold laser energy density for depassivation needs to be determined, as this is most likely to produce the least amount of surface damage. These data, and further development of models which also consider the kinetics of the surface for hydrogen desorption and non-thermal mechanisms for disorder, are needed to develop a physical picture. Second, the spot size of the laser needs to be improved either by bringing fiber-coupled laser light close to the sample surface or utilizing in-chamber optics. The demonstration of photothermal hydrogen patterning in a direct-write mode with energy densities between 75 mJ/cm^2 and 100 mJ/cm^2 indicates that photomask-based desorption can be done on 12” wafers using a reasonable 10 kW laser with a 100 Hz repetition rate. Lastly, while this work focuses on hydrogen desorption from Si (100), the general technique of photothermal modification of near-surface silicon could be

useful more widely for silicon surfaces functionalized with different molecules, ranging from other atom-based resists to different dopant precursors.

5. ACKNOWLEDGEMENTS

This work was supported by the Laboratory Directed Research and Development Program at Sandia National Laboratories, and was performed, in part, at the Center for Integrated Nanotechnologies, a U.S. DOE, Office of Basic Energy Sciences user facility. Sandia National Laboratories is managed and operated by National Technology and Engineering Solutions of Sandia, LLC., a wholly owned subsidiary of Honeywell International, Inc., for the U.S. Department of Energy under contract DE-NA-0003525. The views expressed in the article do not necessarily represent the views of the U.S. DOE or the United States Government.

6. REFERENCES

[1] M. Fuechsle, J. A. Miwa, S. Mahapatra *et al.*, "A single-atom transistor," Nature Nanotechnology, 7(4), 242-246 (2012).

[2] D. Keith, M. G. House, M. B. Donnelly *et al.*, "Single-Shot Spin Readout in Semiconductors Near the Shot-Noise Sensitivity Limit," Physical Review X, 9(4), (2019).

[3] Y. He, S. K. Gorman, D. Keith *et al.*, "A two-qubit gate between phosphorus donor electrons in silicon," Nature, 571(7765), 371-+ (2019).

[4] M. Koch, J. G. Keizer, P. Pakkiam *et al.*, "Spin read-out in atomic qubits in an all-epitaxial three-dimensional transistor," Nature Nanotechnology, 14(2), 137-140 (2019).

[5] D. R. Ward, S. W. Schmuckerm, E. M. Anderson *et al.*, "Atomic Precision Advanced Manufacturing for Digital Electronics," Electronic Device Failure Analysis, 22(1), 4-11 (2020).

[6] T. C. Shen, C. Wang, G. C. Abeln *et al.*, "Atomic-Scale Desorption through Electronic and Vibrational-Excitation Mechanisms," Science, 268(5217), 1590-1592 (1995).

[7] S. R. Schofield, N. J. Curson, M. Y. Simmons *et al.*, "Atomically precise placement of single dopants in Si," Physical Review Letters, 91(13), (2003).

[8] L. Oberbeck, N. J. Curson, T. Hallam *et al.*, "Measurement of phosphorus segregation in silicon at the atomic scale using scanning tunneling microscopy," Applied Physics Letters, 85(8), 1359-1361 (2004).

[9] D. R. Ward, M. T. Marshall, D. M. Campbell *et al.*, "All-optical lithography process for contacting nanometer precision donor devices," Applied Physics Letters, 111(19), (2017).

[10] T. Skeren, N. Pascher, A. Garnier *et al.*, "CMOS platform for atomic-scale device fabrication," Nanotechnology, 29(43), (2018).

[11] T. Hallam, M. J. Butcher, K. E. J. Goh *et al.*, "Use of a scanning electron microscope to pattern large areas of a hydrogen resist for electrical contacts," Journal of Applied Physics, 102(3), (2007).

[12] Z. H. Liu, L. C. Feldman, N. H. Tolk *et al.*, "Desorption of H from Si(111) by resonant excitation of the Si-H vibrational stretch mode (Retracted article. See vol. 333, pg. 1824, 2011)," Science, 312(5776), 1024-1026 (2006).

[13] A. Pusel, U. Wetterauer, and P. Hess, "Photochemical hydrogen desorption from H-terminated silicon(111) by VUV photons," Physical Review Letters, 81(3), 645-648 (1998).

[14] P. Gupta, V. L. Colvin, and S. M. George, "Hydrogen Desorption-Kinetics from Monohydride and Dihydride Species on Silicon Surfaces," Physical Review B, 37(14), 8234-8243 (1988).

[15] J. N. Randall, J. B. Ballard, J. W. Lyding *et al.*, "Atomic precision patterning on Si: An opportunity for a digitized process," Microelectronic Engineering, 87(5-8), 955-958 (2010).

[16] J. Xu, S. H. Overbury, and J. F. Wendelken, "Selective laser removal of the dimer layer from Si(100) surfaces revealed by scanning tunneling microscopy (vol 53, pg R4245, 1996)," Physical Review B, 54(7), 5180-5181 (1996).

[17] J. Kanasaki, M. Nakamura, K. Ishikawa *et al.*, "Primary processes of laser-induced selective dimer-layer removal on Si(001)-(2 x 1)," Physical Review Letters, 89(25), (2002).

[18] K. Yasui, and J. Kanasaki, "Scanning tunneling microscopic studies of laser-induced modifications of Si(001)-(2x1) surface," Journal of Applied Physics, 110(10), (2011).

[19] D. P. Korfiatis, K. A. T. Thoma, and J. C. Vardaxoglou, "Conditions for femtosecond laser melting of silicon," Journal of Physics D-Applied Physics, 40(21), 6803-6808 (2007).

[20] C. K. Ong, E. H. Sin, and H. S. Tan, “Heat-Flow Calculation of Pulsed Excimer Ultraviolet-Lasers Melting of Amorphous and Crystalline Silicon Surfaces,” Journal of the Optical Society of America B-Optical Physics, 3(5), 812-814 (1986).
[21] G. E. Jellison, and F. A. Modine, “Optical Functions of Silicon between 1.7 and 4.7 Ev at Elevated-Temperatures,” Physical Review B, 27(12), 7466-7472 (1983).
[22] A. E. Bell, “Review and Analysis of Laser Annealing,” Rca Review, 40(3), 295-338 (1979).